PHYSICAL REVIEW B VOLUME 21, NUMBER 9 1 MAY 1980

Calculations of the dynamic susceptibility of nickel and iron

J. F. Cooke, J. W. Lynn,* and H. L. Davis
Solid State Division, Oak Ridge National Laboratory, Oak Ridge, Tennessee 37830
(Received 26 October 1979)

The spin dynamics of the transition-metal ferromagnets nickel and iron are investigated within the framework of the itinerant theory of magnetism. The theory is developed in terms of a generalized random-phase approximation which incorporates the band and wave-vector dependence of relevant interaction matrix elements. In contrast to constant-matrix-element approximations, this formalism generates band- and wave-vector-dependent splitting of the energy bands, possible "optical" spin-wave modes, and a different interpretation of the spin-wave disappearance phenomena. First-principles numerical calculations of the neutron scattering intensity based on this model have been found to be in excellent agreement with experiments. Recent neutron scattering experiments have also verified the existence of an "optical" spin-wave branch predicted by this theory.

I. INTRODUCTION

The itinerant (or band) model of magnetism is known to provide a good qualitative description of the one-electron properties of transition-metal magnets. For example, well-defined Fermi surfaces, nonintegral magnetic moments, the known *d*-electron contribution to the specfic heat, high-field susceptibility, and x-ray photoemission are all consistent with the concept of electrons occupying energy bands and, consequently, free to move through the lattice.[1] The development of a reasonably accurate theory which is also amenable to numerical investigation is, however, a very difficult task. In addition to the well-known problems associated with conventional energy-band theory, the complicated exchange and correlation effects between opposite-spin electrons must be treated since they are of fundamental importance to the itinerant theory of magnetism. It is not too surprising, therefore, that the vast majority of work on the itinerant model has been in the area of developing theories and techniques for calculating one-electron energies and wave functions.

In order to test the results of these "first-principles" calculations comparisons are usually made with experimental results relating to one-electron properties of the magnet. While these comparisons are certainly useful in testing the validity of the theory a more detailed and stringent criterion is to test whether the theory can provide a satisfactory description of the spin dynamics, i.e., the dynamic susceptibility $\chi(\vec{q}, \omega)$. This function contains all of the relevant information about the dynamics of the spin system and can be directly measured by inelastic neutron scattering experiments.

Such neutron experiments have provided direct information about the elementary excitations of magnetic systems, the spin waves. Of particular interest for itinerant magnets is the qualitative prediction that spin waves may not exist over the full Brillouin zone.[2] The subsequent observation of the disappearance of the spin-wave mode in both ferromagnetic nickel[3] and iron[4] not only verified this unique prediction of the itinerant model but has provided the stimulus to perform first-principles calculations. Such calculations can provide a sensitive test of the itinerant formalism because the behavior of the spin-wave dispersion curve as well as the disappearance phenomenon depend directly on the details of band structure.

Realistic numerical calculations of $\chi(\vec{q}, \omega)$ are not easy to carry out since they need as input the electronic energy bands, wave functions, and relevant interaction matrix elements. Several attempts have been made to calculate $\chi(\vec{q}, \omega)$ by employing certain simplifying assumptions. The first calculation of this type was performed by Thompson[5] using a parametrized single-parabolic-band description for nickel's electronic structure. This model proved inadequate because of the oversimplification of the band structure. The first attempt to use realistic energy bands for nickel in the calculation of its susceptibility was undertaken by Lowde and Windsor.[6] They calculated $\chi(\vec{q}, \omega)$ using the random-phase approximation (RPA) and rigidly spin-split bands. Again the agreement between theory and experiment was not very good.

It is important to note here that Lowde and Windsor's RPA calculations were based on matrix-element approximations which we feel are not appropriate for transition-metal systems. Their approximation neglected all of the band and wave-vector dependence of relevant matrix elements which, as will be shown below, significantly affects the calculation. Several years ago Cooke[7] suggested an approximate way to include the band and wave-vector

dependence of these matrix elements provided the spin dependence of the electronic wave functions could be neglected. It was shown that the improved matrix-element approximation not only led to an altered expression for the RPA susceptibility but introduced a new effect, a wave-vector-dependent splitting of the electronic energy bands. During the past few years we have carried out an extensive first-principles numerical investigation of this improved RPA formalism and have found excellent agreement with the neutron scattering results for both nickel and iron. Some of these results have been reported previously in the literature.[8]

The purpose of this paper is twofold. The first objective is to generalize the original work of Cooke to incorporate self-consistent spin-polarized wave functions into the theory, while retaining the essential physical criterion that the spin-wave energy approaches zero as $\vec{q} \to 0$ (Goldstone theorem). The second objective is to bring together and unify the numerical results which have been obtained thus far for ferromagnetic nickel and iron. We will also present and discuss some new results for $\chi(\vec{q},\omega)$ and the Stoner density of states obtained from several different band calculations.

II. GENERAL THEORY

The basic assumption of the itinerant theory of magnetism is that, at least to first order, the electrons which are responsible for the magnetic properties of a system occupy energy bands and propagate through the crystal. We choose, therefore, to write the general Hamiltonian in terms of a complete set of Bloch states $\{\psi_{n\vec{k}\sigma}(\vec{r})\}$, where n is the band index, $\vec{k}$ is the wave vector, and σ is the electron spin. If we define $C^{\dagger}_{n\vec{k}\sigma}$ and $C_{n\vec{k}\sigma}$ as creation and destruction operators, respectively, for electrons in the state $\psi_{n\vec{k}\sigma}$ then

$$H = \sum_{n,m,\vec{k},\sigma} (n\vec{k}\sigma \left| -\frac{\hbar^2\nabla^2}{2m_e} + U(\vec{r}) \right| m\vec{k}\sigma)\, C^{\dagger}_{n\vec{k}\sigma} C_{m\vec{k}\sigma}$$
$$+ \frac{1}{2} \sum_{\substack{n_1,n_2,n_3,n_4,\\ \vec{k}_1\vec{k}_2\vec{k}_3,\sigma,\sigma'}} (n_1\vec{k}_1\sigma, n_2\vec{k}_2\sigma' \left| \frac{e^2}{|\vec{r}-\vec{r}'|} \right| n_3\vec{k}_3\sigma', n_4\vec{k}_1 + \vec{k}_2 - \vec{k}_3\sigma)\, C^{\dagger}_{n_1\vec{k}_1\sigma} C^{\dagger}_{n_2\vec{k}_2\sigma'} C_{n_3\vec{k}_3\sigma'} C_{n_4\vec{k}_1+\vec{k}_2-\vec{k}_3\sigma} \quad , \tag{1}$$

where $U(\vec{r})$ is the electron-nuclear interaction.

It can be shown that both the magnetic susceptibility and the spin-only part of the inelastic neutron scattering intensity can be uniquely determined from the time Fourier transform to the spin-spin correlation function $\langle S^{\alpha}_{\vec{q}}(t) S^{\beta}_{-\vec{q}}(0)\rangle$, where S^{α} is the α component of the spin operator S.[9] This correlation function can in turn be obtained directly from the Green's function

$$G_{\alpha\beta}(\vec{q},t) = -i\langle T S^{\alpha}_{\vec{q}}(t) S^{\beta}_{-\vec{q}}(0)\rangle \quad , \tag{2}$$

where T is the time-ordering operator. Therefore, the problem of calculating the dynamics of the spin system can be reduced to a calculation of the Green's function defined in Eq. (2).

Information about the spin-waves is contained in the transverse Green's function[7]

$$G_{\rm sw}(\vec{q},t) = -i\langle T S^{-}_{\vec{q}}(t) S^{+}_{-\vec{q}}(0)\rangle \quad , \tag{3}$$

where

$$S^{\pm}_{\vec{q}} = S^{x}_{\vec{q}} \pm i S^{y}_{\vec{q}} \tag{4}$$

are the spin-ladder operators. The imaginary part of the time transform of $G_{\rm sw}(\vec{q},t)$ is in essence the imaginary part of the dynamic susceptibility $\chi(\vec{q},\omega)$, and hence is directly related to the neutron scattering cross section. If the spin-waves correspond to true eigenstates of the Hamiltonian then they will appear as δ-function singularities in $\chi(\vec{q},\omega)$. If, however, a spin-wave of wave vector $\vec{q}$ has available some decay mechanism such as a spin-flip (Stoner) excitation, then the magnetic response at that wave vector will be distributed over a range of frequencies. Indeed with a sufficiently large decay probability the response will be spread over such a large range that the spin-wave will no longer exist as a well defined entity. The remainder of this paper will be devoted to an approximate determination and subsequent numerical evaluation of Eq. (3). The remainder of the Green's-function matrix-element, $G_{\alpha\beta}$, can also be determined but those results will not be given here.

In order to determine $G_{\rm sw}$ we first write it in terms of electron creation and destruction operators. This can be done by using the second quantization form for $S^{-}_{\vec{q}}$,

$$S^{-}_{\vec{q}} = \sum_{nm,\vec{k}} (n\vec{k}\downarrow | e^{-i\vec{q}\cdot\vec{r}} | m\vec{k}+\vec{q}\uparrow)\, C^{\dagger}_{n\vec{k}\downarrow} C_{m\vec{k}+\vec{q}\uparrow} \quad . \tag{5}$$

Substitution of this result into Eq. (3) gives

$$G_{\rm sw}(\vec{q},t) = \sum_{n,m,\vec{k}} (n\vec{k}\downarrow | e^{-i\vec{q}\cdot\vec{r}} | m\vec{k}+\vec{q}\uparrow) \times G_2(n\vec{k}, m\vec{k}+\vec{q}, t) \quad , \tag{6}$$

where

$$G_2(n\vec{k},m\vec{k}+\vec{q},t) = -i\langle TC^{+}_{n\vec{k}\downarrow}(t)C_{m\vec{k}+\vec{q}\uparrow}(t)S^{+}_{-\vec{q}}(0)\rangle \quad . \quad (7)$$

We solve for G_2 by using the equation of motion method which generates an infinite set of equations coupling G_2 to higher-order Green's functions. We now introduce the well-known RPA decoupling scheme in the equation for G_2.[7,8] This approximation limits the theory to low temperature because it neglects spin-wave–spin-wave interactions, as well as certain spin-wave–electron and electron-electron interactions.

The equation for G_2 which results from this decoupling scheme can be further simplified by requiring that the Bloch functions satisfy the following equation:

$$\left[-\frac{\hbar^2\nabla^2}{2m_e}+U(\vec{r})+\sum_{m\vec{p}\alpha} f_{m\vec{p}\alpha}\int \bar{\psi}_{m\vec{p}\alpha}(\vec{r}')\frac{e^2}{|\vec{r}-\vec{r}'|}\psi_{m\vec{p}\alpha}(\vec{r}')\,d^3r'\right]\psi_{n\vec{k}\sigma}(\vec{r}) - \sum_{m\vec{p}} f_{m\vec{p}\sigma}\psi_{m\vec{p}\sigma}(\vec{r})\int \bar{\psi}_{m\vec{p}\sigma}(\vec{r}')U_{sc}(\vec{r},\vec{r}')\psi_{n\vec{k}\sigma}(\vec{r}')\,d^3r' = E(n\vec{k}\sigma)\psi_{n\vec{k}\sigma}(\vec{r}) \quad , \quad (8)$$

where $f_{n\vec{k}\sigma}$ is the Fermi occupation number, $E(n\vec{k}\sigma)$ is the electronic energy, and $U_{sc}(\vec{r},\vec{r}')$ is a self-consistently screened electron-electron interaction. The determination of a realistic $U_{sc}(\vec{r},\vec{r}')$ which contains all of the relevant exchange and correlation effects is the most important, and most difficult, problem associated with the energy-band calculations. We will return to this point later.

For the moment we assume that Eq. (8) can be solved for the electronic energies and wave functions. The equation for the time Fourier transform of G_2 then reduces to

$$[z-E(m\vec{k}+\vec{q}\uparrow)+E(n\vec{k}\downarrow)]G_2(n\vec{k},m\vec{k}+\vec{q},z)=\hbar(m\vec{k}+\vec{q}\uparrow|e^{i\vec{q}\cdot\vec{r}}|n\vec{k}\downarrow)(f_{n\vec{k}\downarrow}-f_{m\vec{k}+\vec{q}\uparrow})-(f_{n\vec{k}\downarrow}-f_{m\vec{k}+\vec{q}\uparrow}) \times\sum_{i,j,\vec{p}}(m\vec{k}+\vec{q}\uparrow i\vec{p}\downarrow|U_{sc}(\vec{r},\vec{r}')|n\vec{k}\downarrow j\vec{p}+\vec{q}\uparrow)G_2(i\vec{p},j\vec{p}+\vec{q},z) \quad . \quad (9)$$

Because of the approximations made to this point, Eqs. (8) and (9) represent the general RPA result for the itinerant theory. One important feature of these equations is that the Goldstone theorem is preserved no matter what we use for U_{sc}. This result follows as an indentity which can be obtained from Eq. (8). If we multiply Eq. (8) through by $\bar{\psi}_{m\vec{k}\sigma'}(\vec{r})$ and integrate on $\vec{r}$ it is straightforward to show that

$$E(n\vec{k}\sigma)(m\vec{k}\sigma'|n\vec{k}\sigma)=(m\vec{k}\sigma'\left|-\frac{\hbar^2\nabla^2}{2m_e}+U(\vec{r})\right|n\vec{k}\sigma)+\sum_{i\vec{p}\alpha}(i\vec{p}\alpha,m\vec{k}\sigma'\left|\frac{e^2}{|\vec{r}-\vec{r}'|}\right|n\vec{k}\sigma,i\vec{p}\alpha)f_{i\vec{p}\alpha} - \sum_{i\vec{p}}(i\vec{p}\sigma,m\vec{k}\sigma'|U_{sc}(\vec{r},\vec{r}')|i\vec{p}\sigma,n\vec{k}\sigma)f_{i\vec{p}\sigma} \quad . \quad (10)$$

If $\vec{q}=0$ is inserted in Eq. (9) and the result given by Eq. (10) is used together with the completeness property of the $\{\psi_{m\vec{k}\sigma}(\vec{r})\}$, then

$$G_{sw}(\vec{q}=0,z)=\hbar[(n_\downarrow-n_\uparrow)/z] \quad . \quad (11)$$

This result is in fact exact and simply states that the only pole in G_{sw} at $\vec{q}=0$ is at $z=0$. This pole must correspond to the spin-wave pole and, therefore, the spin-wave energy must vanish as $\vec{q}\to 0$.

In order to solve Eqs. (8) and (9) for the general case we must first determine the relevant interaction matrix elements. Since U_{sc} is not known exactly we must rely on approximate expressions. The simplest approximation is to ignore all of the band and wave-vector dependence of these matrix elements. If we consider only the "d bands" and replace the interaction matrix element in Eq. (9) by a constant then the equation can be solved to yield the enhanced susceptibility expression used by Lowde and Windsor.[6] In addition, we see from Eq. (8) that if the spin dependence of the wave functions is neglected then this approximation also leads to a rigid splitting of the electronic energy bands $[E(n\vec{k}\uparrow)-E(n\vec{k}\downarrow)=\text{const}]$. By further simplifying these results to the case of a single parabolic band we recover the result investigated by Thompson.[5]

It is important to notice here that this enhanced-susceptibility–rigid-band-splitting model is an approximate solution of the general RPA equations which is valid only in the constant-matrix-element limit. For systems such as the 3-d transition-metal series where the band and wave-vector dependence of the U_{sc} matrix element may be important we must find a more realistic solution. Incorporation of these effects into the theory requires some detailed knowledge of the

electronic wave functions.

Consider the Korringa-Kohn-Rostocker (KKR) form of the wave function[10]

$$\psi_{n\vec{k}\sigma}(\vec{r}) = \sum_{\mu} a_{n\mu\sigma}(\vec{k})\phi_{\mu}^{\sigma}(\vec{r}), \quad |\vec{r}| < R_{\mathrm{MT}} , \tag{12}$$

where the ϕ_{μ}^{σ} are products of radial functions and real spherical harmonics, the $a_{n\mu\sigma}(\vec{k})$ are expansion coefficients, R_{MT} is the muffin-tin radius, and μ is a symmetry index which corresponds to the angular momentum indices (lm). If we extrapolate this wave function out to the unit cell boundary and neglect the relatively small energy and spin dependence of the radial functions then

$$\begin{aligned}(n_1\vec{k}_1\sigma n_2\vec{k}_2\sigma'|U_{\mathrm{sc}}|n_3\vec{k}_3\sigma' n_4\vec{k}_4\sigma) &= \sum_{\substack{\mu\nu \\ \eta\xi}} a_{n_1\mu\sigma}(\vec{k}_1)a_{n_2\nu\sigma'}(\vec{k}_2) \\ &\times a_{n_3\eta\sigma'}(\vec{k}_3)a_{n_4\xi\sigma}(\vec{k}_4)W_{\eta\mu\nu\xi} , \end{aligned} \tag{13}$$

where W is a matrix element of U_{sc} calculated with respect to the symmetry orbitals ϕ_{μ}.

The other matrix element in Eq. (9) can be treated in a similar way to yield

$$\begin{aligned}(n\vec{k}\sigma|e^{-i\vec{q}\cdot\vec{r}}|m\vec{k}+\vec{q}\sigma') &= \sum_{\mu\nu} a_{n\mu\sigma}(\vec{k})a_{m\nu\sigma'}(\vec{k}+\vec{q})F_{\mu\nu}(\vec{q}) , \end{aligned} \tag{14}$$

where

$$F_{\mu\nu}(\vec{q}) = \int \bar{\phi}_{\mu}(\vec{r})e^{-i\vec{q}\cdot\vec{r}}\phi_{\nu}(\vec{r})\,d^3r . \tag{15}$$

The integral in Eq. (15) extends over the unit cell.

Because of the separation of variables generated by the expansion coefficients, substitution of the expansions given in Eqs. (13) and (14) into Eq. (9) allows us to convert the equation for G_2 into a matrix equation which can be solved. Then, from Eq. (6), we find

$$\begin{aligned}G_{\mathrm{sw}}(\vec{q},z) &= \sum_{LL',L''} F_L(\vec{q})[I+\Gamma(\vec{q},z)W]^{-1}_{LL'} \\ &\times \Gamma_{L',L''}(\vec{q},z)F^*_{L''}(\vec{q}) , \end{aligned} \tag{16}$$

where the pair of symmetry indices (μ,ν) has been replaced by a single index L which runs over all possible combinations, I is the unit matrix, and

$$\Gamma_{L,L'}(\vec{q},z) = \Gamma_{\mu\nu,\eta\xi}(\vec{q},z) = \frac{1}{N}\sum_{nm,\vec{k}} \frac{a_{n\mu\downarrow}(\vec{k})a_{m\nu\uparrow}(\vec{k}+\vec{q})a_{n\eta\downarrow}(\vec{k})a_{n\xi\uparrow}(\vec{k}+\vec{q})(f_{n\vec{k}\downarrow}-f_{m\vec{k}+\vec{q}\uparrow})}{z-E(m\vec{k}+\vec{q}\uparrow)+E(n\vec{k}\downarrow)} . \tag{17}$$

The result given in Eq. (16) represents the general RPA solution under the assumptions made about the wave functions. The inclusion of the band and wave-vector dependence of the matrix elements has led to a more complicated result than the enhanced susceptibility expression considered by Lowde and Windsor.[6] Another important aspect of this solution is that because of the matrix character of the solution we have the possibility of more than one spin-wave mode. The existence and number of such additional modes depends on the details of the band structure.

III. ONE-ELECTRON PROPERTIES

In this section we will investigate the effect of including the band and wave-vector dependence of the interaction matrix elements on the energy-band structure. By substituting the result given in Eq. (13) into Eq. (10) we find that the electronic energy can be written in the general form

$$\begin{aligned}E(n\vec{k}\sigma) &= \epsilon(n\vec{k}\sigma) + \sum_{\mu,\nu} a_{n\mu\sigma}(\vec{k})a_{n\nu\sigma}(\vec{k}) \\ &\times (h^{\sigma}_{\mu,\nu} - h^{p}_{\mu,\nu}) , \end{aligned} \tag{18}$$

with

$$h^{\sigma}_{\mu,\nu} = \sum_{\eta} W_{\mu\nu,\eta\eta}f_{\eta,\sigma} \tag{19}$$

and

$$f_{\mu,\sigma} = \frac{1}{N}\sum_{m\vec{p}} |a_{m\mu\sigma}(\vec{p})|^2 f_{m\vec{p}\sigma} . \tag{20}$$

Here $\epsilon(n\vec{k}\sigma)$ is the contribution from the first two terms on the right-hand side of Eq. (10). This contribution has a very weak spin dependence generated by the explicit spin dependence of the wave functions. Essentially all of the spin dependence of the electronic energy comes from the second term in Eq. (18). The function $h^{p}_{\mu,\nu}$ is just $h^{\sigma}_{\mu,\nu}$ evaluated in the "paramagnetic state," i.e., the nonmagnetic state. In this case the wave functions are not spin dependent and the electronic energy reduces to $\epsilon(n\vec{k}\uparrow) = \epsilon(n\vec{k}\downarrow)$. The function $f_{\mu,\sigma}$ is just the number of electrons of symmetry type μ and spin σ.

The spin-splitting parameter Δ is defined by

$$\Delta(n,\vec{k}) = E(n\vec{k}\uparrow) - E(n\vec{k}\downarrow) \tag{21}$$

and from Eq. (18) we see that it is both band and wave-vector dependent, in contrast to the constant-

matrix-element result where Δ is a constant. Notice also that the splitting depends on a sum of the number of electrons with a given symmetry index weighted by the relevant interaction matrix element, and not simply on the total number of electrons with a given spin.

The procedure we use to obtain the band structure for an itinerant magnet is based on a perturbation approach. The first step is to carry out a conventional nonmagnetic band calculation for the system of interest. These results are then used as the starting point for a self-consistent calculation of the spin-polarized bands and wave functions. By doing the calculation in this manner we need only consider the parameters $W_{\mu\nu\eta\xi}$ in terms of how they effect the spin-dependent part of the calculation. This will allow us to reduce the number of parameters needed in the theory considerably.

For example, first-principles spin-polarized calculations indicate that the spin splitting of the s- and p-like states is very small compared to the d-like states[11] and so, as a first approximation, we retain only those $W_{\mu\nu\eta\xi}$ which refer to d symmetry. Furthermore, we retain only the diagonal terms $W_{\mu\mu\mu\mu} = W_\mu$, and assume that the W_μ are identical for all μ belonging to the same irreducible representation. Based on these assumptions the electronic energy reduces to

$$E(n\vec{k}\sigma) = \epsilon(n\vec{k}\sigma) + \sum_{\mu}{}' |a_{n\mu\sigma}(\vec{k})|^2 (h^{\sigma}_{\mu,\mu} - h^{p}_{\mu,\mu}) , \tag{22}$$

where $\sum'$ refers to a sum only over d-symmetry terms and

$$h^{\sigma}_{\mu,\mu} = W_\mu f_{\mu,\sigma} . \tag{23}$$

There are five terms in the sum in Eq. (22) but only two parameters, corresponding to e_g and t_{2g} representations. This result is similar in form to the energy expression obtained from the Hodges, Ehrenreich, and Lang interpolation scheme[12] provided we neglect the (weak) spin dependence of $\epsilon(nk\sigma)$ and replace the W_μ by a single constant.

There are several ways to proceed with the calculation. One method, outlined previously by Cooke,[8] is to make use of Slater-Koster[13] (for bcc iron) or Hodges, Ehrenreich, and Lang[12] (for fcc nickel) to set up a self-consistent procedure for obtaining the spin-polarized bands and wave-function expansion coefficients. This procedure is not only applicable to our perturbation approach but can also, in principle, be modified to allow us to calculate the dynamics of a magnet from any given band structure.

Self-consistent calculations have been carried out using this formalism for ferromagnetic nickel and iron. These calculations indicate that the spin dependence of the wave functions can be neglected without introducing significant errors, which implies that in Eq. (22) we can neglect the spin dependence of $\epsilon(n\vec{k}\sigma) \rightarrow \epsilon(n\vec{k})$ and $a_{n\mu\sigma}(\vec{k}) \rightarrow a_{n\mu}(\vec{k})$. This result suggests an alternative approach to calculating the spin-polarized band structure without having to use any interpolation scheme; determine $\epsilon(n\vec{k})$ and $a_{n\mu}(\vec{k})$ from a "realistic" KKR calculation for the paramagnetic state and then iterate Eqs. (22) and (23) to convergence for fixed parameters W_μ. We have found essentially the same spin-polarized band structure from both techniques outlined above. It must be emphasized, however, that while the calculations presented in this paper are not sensitive to the spin dependence of the electronic wave functions this is not necessarily true for other types of calculations, e.g., the magnetic form factor.

We thus have two parameters, $W_{t_{2g}}$ and W_{e_g}, at our disposal. These two parameters have been chosen so that the calculated ferromagnetic band structure gives the observed magnetic moment, and the correct t_{2g} to e_g character of the moment as observed in neutron magnetic form-factor measurements. For nickel the spin-only moment[14,15] (at $T = 0$ K) was taken to be $0.561\mu_B$, with 19% e_g character to the moment,[16] while for iron[14,15] $\mu_{\text{spin}} = 2.122\mu_B$, with 53% e_g character to the moment.[17] Consequently once the paramagnetic band

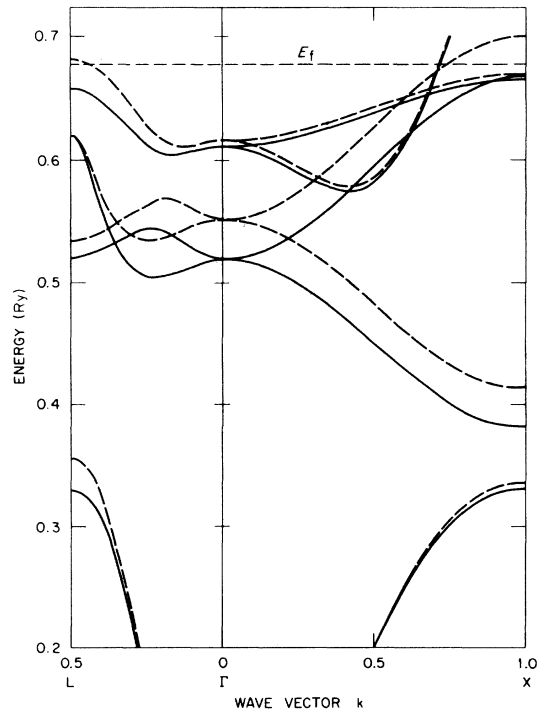

FIG. 1. Ferromagnetic energy bands generated from Stocks's *et al.* (Ref. 18) paramagnetic potential. The solid curves are for the majority spin while the dashed curves are for the minority spin.

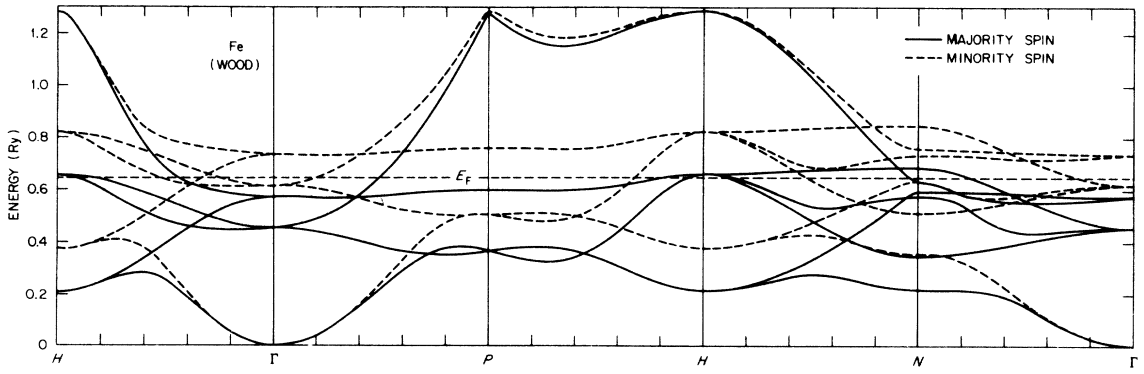

FIG. 2. Ferromagnetic energy bands for iron generated from Wood's (Ref. 22) paramagnetic potential.

structure has been chosen, the only two adjusted parameters in the theory are fixed by the basic static quantities know about the moment, and thus *there are no adjustable parameters available in the calculations of the dynamic susceptibility to force agreement with the inelastic neutron scattering experiments.*

The ferromagnetic band structure of nickel, based on the paramagnetic bands proposed by Stocks *et al.*[18] is shown in Fig. 1. The spin splitting of the *d*-like bands is strongly wave-vector dependent as a result of the different splittings obtained for the e_g and t_{2g} symmetries; i.e., $\Delta_{t_{2g}} \simeq 0.4$ eV and $\Delta_{e_g} \simeq 0.1$ eV. Additional wave-vector-dependent splitting results from *spd* hybridization. Because of the relatively small e_g splitting we find only one hole pocket at the X point, in agreement with experiment.[19] This is quite different from most other calculations[20] which find $\Delta_{e_g} \cong \Delta_{t_{2g}}$ and two hole pockets at X. The results of this band calculation are also in good agreement with the recent angular resolved photoemission results obtained by Eastman *et al.*[21] In particular, the calculated spin splitting at the L point is approximately 0.3 eV, which is in agreement with the experiments and half as big as predicted by other calculations.[20]

The results for iron differ from nickel in that the t_{2g} and e_g splittings needed to produce the correct symmetry character of the moment turn out to be essentially identical, which leads to an approximate rigid splitting of the *d*-like bands. The wave-vector dependence of the band splitting in this case originates solely from the *sp* hybridization of the *d* bands; the splitting at each $\vec{k}$ is then proportional to the amount of *d* character of the band at that $\vec{k}$. Figure 2 shows the ferromagnetic band structure generated from Wood's paramagnetic band structure.[22] Slater-Koster parameters out to second-nearest neighbors (resulting in 27 parameters) were used to fit to Wood's bands, and the parameters found were similar to the values used by Gold *et al.*[23] The conditions on the moment were then used to generate the ferromagnetic band structure.

A number of other band structures were also used to calculate the one-electron properties (and dynamic susceptibility) taken from both KKR first-principles calculations as well as from paramagnetic and ferromagnetic band structures taken from the literature.[24–27] The ferromagnetic band structures[26,27] were handled by fitting the Slater-Koster parameters to the spin-up and spin-down bands separately. By way of example we show in Fig. 3 the total density of electron states calculated from Wood's potential, and

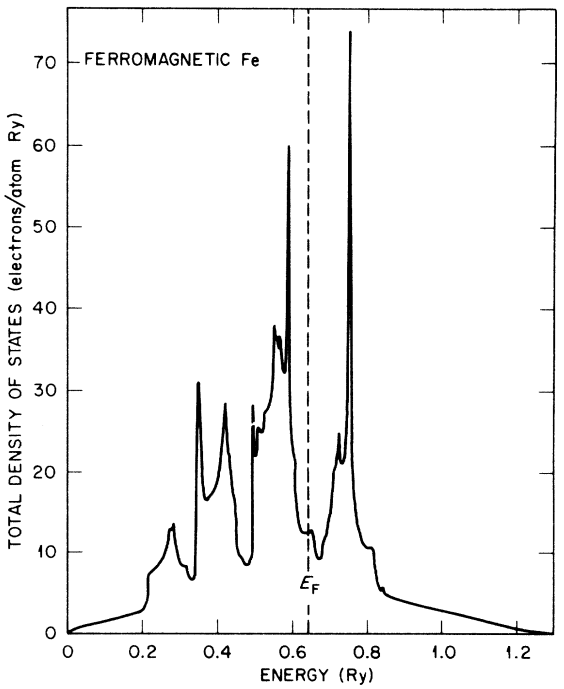

FIG. 3. Total density of states for ferromagnetic iron.

Fig. 4 shows the projected density of states for e_g, t_{2g}, and *sp* character for majority spin states (solid curve) and minority spin states (dashed curve). Note that due to the *spd* hybridization the splitting does not correspond to a rigid shifting of the majority and minority densities of states. The areas below the Fermi energy for the symmetry projected curves give the total number of electrons of the symmetry and spin type, $f_{\mu,\sigma}$. Addition of these symmetry projected curves gives, of course, the total density of states shown in Fig. 3. These calculations have been done using the Gilat-Raubenheimer (GR)[28] technique, with a mesh of 3080 $\vec{k}$ points in the $\frac{1}{48}$ irreducible Brillouin zone (BZ) and an energy mesh of 0.000 68 Ry. These calculations were not particularly time consuming, and the fine mesh assured very accurate numerical convergence. For this example we obtained the following: $\mu(t_{2g})=1.406\mu_B$, $\mu(e_g)=1.777\mu_B$, $\mu(sp)=-0.100\mu_B$, $E_F=0.6442$ Ry (measured from the bottom of the bands), and $\Delta=2.22$ eV. This gives a total spin-only moment of $2.123\mu_B$, and the net *d* spin a 52.9% character as observed experimentally.[17] At the Fermi surface we find that the electrons are characterized by having 80% t_{2g} character and 76% majority spin. We remark that the small oppositely directed "conduction-electron" moment results solely from *spd* hybridization effects and not from exchange effects. A small negative conduction-electron moment is observed experimentally.[16,17] Corresponding results for nickel were also obtained but will not be given here.

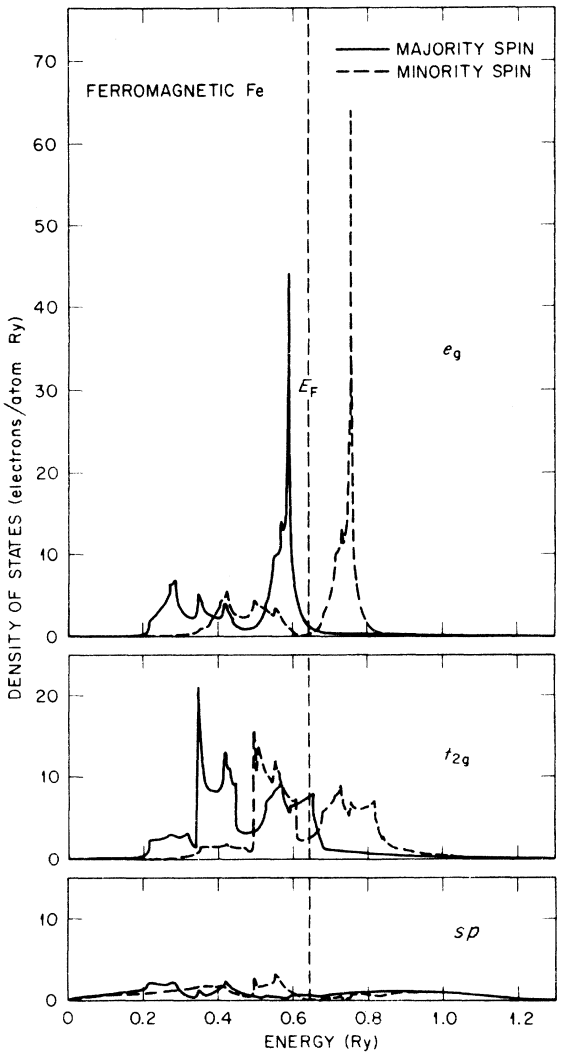

FIG. 4. Symmetry projected density of states for iron.

The band structures presented in this section are not intended to be correct in every detail but we feel they are reasonable. The Fermi surfaces are reasonably correct, as guaranteed by the use of realistic paramagnetic bands, and the moment and symmetry character of the moment are also correct, as guaranteed by the choice of the two parameters in the theory. In the next section we will use these band structures to calculate the dynamic properties of the spin system within the RPA.

IV. CALCULATIONS OF THE DYNAMIC SUSCEPTIBILITY

The general form of the solution for G_{sw} given in Eq. (16) is not altered by the approximations we have made for W. Numerical calculations of the $F_{\mu\nu}$ which appear in this equation have demonstrated that, to reasonable approximation, we need only consider the diagonal terms in the calculation of G_{sw}. In addition the *s* and *p* contributions have also been shown by direct numerical calculation to be negligibly small in comparison to the *d*-symmetry terms. Therefore, to a reasonable numerical approximation, the major contribution to G_{sw} is

$$G_{sw}(\vec{q},z)=\sum_{\mu}{}' F_{\mu,\mu}(\vec{q})[I+\Gamma(\vec{q},z)W]^{-1}_{\mu\nu} \times \Gamma_{\nu\eta}(\vec{q},z)F^{*}_{\eta,\eta}(\vec{q}) \ , \qquad (24)$$

where, again, the prime on the sum indicates a sum over only the *d*-symmetry indices, and

$$[\Gamma(\vec{q},z)W]_{\mu\nu}=\Gamma_{\mu\mu,\nu\nu}(\vec{q},z)W_{\nu} \ . \qquad (25)$$

Notice that the only parameters which appear in the expression for G_{sw} are the same two which were fixed by the requirement that the band structure yield the correct moment and ratio of e_g to t_{2g} character in the moment. *Thus, in this model the dynamics of the spin system is uniquely determined from the band structure; i.e., there are no adjustable parameters.*

An extensive series of first-principles calculations of G_{sw} has been carried out for nickel and iron. The initial calculations published some years ago for nick-

el were obtained using the Gilat-Raubenheimer[28] technique for calculating the BZ sums defined in Eq. (17) and paramagnetic wave-function expansion coefficients. Since that time new computer programs based on the tetrahedron BZ integration method[29] and spin-polarized expansion coefficients have been developed and applied to the calculation of G_{sw}. The tetrahedron method is, in principle, a better technique for calculating BZ sums like the ones encountered in this problem because, unlike the GR scheme, it can treat exactly the Fermi factor difference $f_{n\vec{k}\downarrow} - f_{n\vec{k}+\vec{q}\uparrow}$. We found, however, that both techniques gave essentially the same results if carried to numerical convergence.

The results presented here will be in terms of the spin-only part of the transverse inelastic neutron cross section for scattering neutrons into the solid angle $d\Omega$, which for low temperatures[9] is proportional to the imaginary part of G_{sw}

$$\left.\frac{d^2\sigma}{d\Omega\, d\omega}\right|_T \sim \lim_{\epsilon\to 0}[\mathrm{Im}G_{sw}(\vec{q},\omega+i\epsilon)] \ . \qquad (26)$$

All of the calculations were carried out for zero temperature since the theory is valid only in this limit. The 12 lowest-energy bands were used, 6 majority and 6 minority.

The scattering cross section for iron for various values of $\vec{q}$ along [100] is shown in Fig. 5. The results along the [110] and [111] were found to be virtually the same as along [100]. The spin-wave dispersion curve obtained from the position of the spin-wave peaks is found to be isotropic in $\vec{q}$ and is plotted in Fig. 6. The agreement with the experimental results[4] is seen to be excellent.

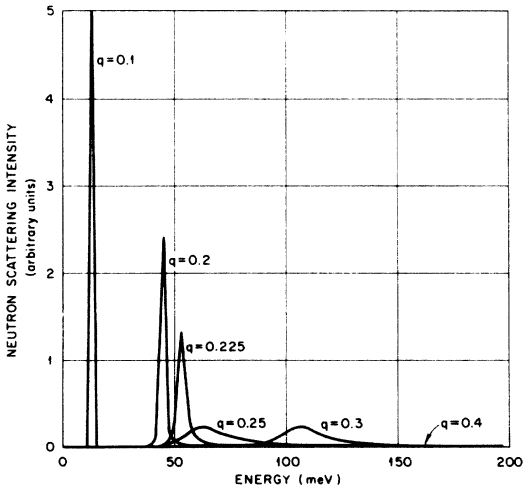

FIG. 5. Spin-wave scattering cross section for ferromagnetic iron for various wave vectors (in units of $2\pi/a_0$) along [100]. The area under each curve for the individual $\vec{q}$'s is a constant.

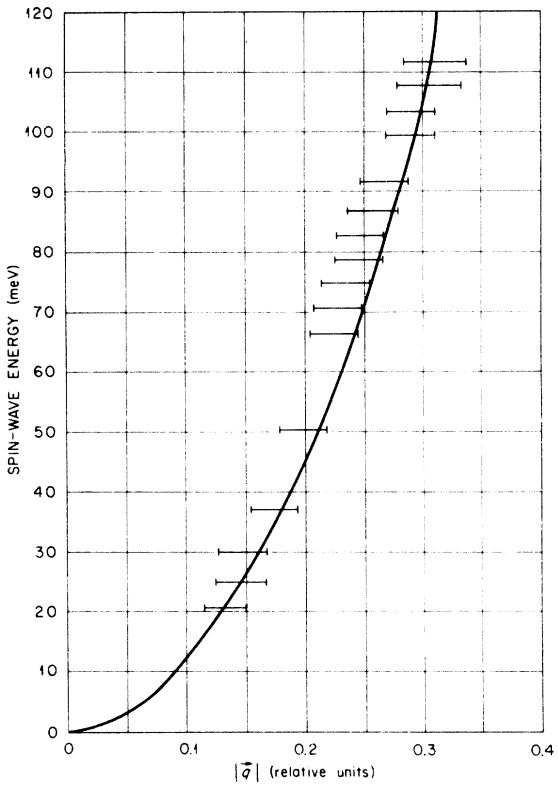

FIG. 6. Spin-wave dispersion curve for ferromagnetic iron. The solid curve represents the present work, while the bars are experimental values at room temperature from Ref. 4.

As the spin-wave peak increases in energy at the higher $|\vec{q}|$, the magnitude of the peak decreases as the width increases. The area under the curve however, remains constant; that is

$$\int [\mathrm{Im}G_{sw}(\vec{q},\omega)]\, d\omega = C \ , \qquad (27)$$

where C is a constant. Thus the "disappearance" of the spin-wave scattering in the neutron scattering experiments in actuality depends solely on the instrumental resolution and sensitivity. For the resolution used in the experiments[3,4] [$\sim 15 \rightarrow 20$ meV FWHM (full width at half maximum) at spin-wave energies ~ 100 meV] we see that the calculations would predict little change in the integrated intensity of the scattering (as measured at constant ω, not constant $\vec{q}$) until a spin-wave energy of ~ 70 meV, where the spin-wave linewidth becomes comparable to the instrumental resolution. The measured intensity would then gradually decrease as the intrinsic linewidth increased until the scattering became undetectable. Between $q = 0.35$ and 0.40 we find that the spin-wave linewidth increases substantially, and in addition a second spin-wave peak is clearly evident at ~ 360 meV as shown in Fig. 7. The peak intensity of this scattering is very weak compared with the spin-wave

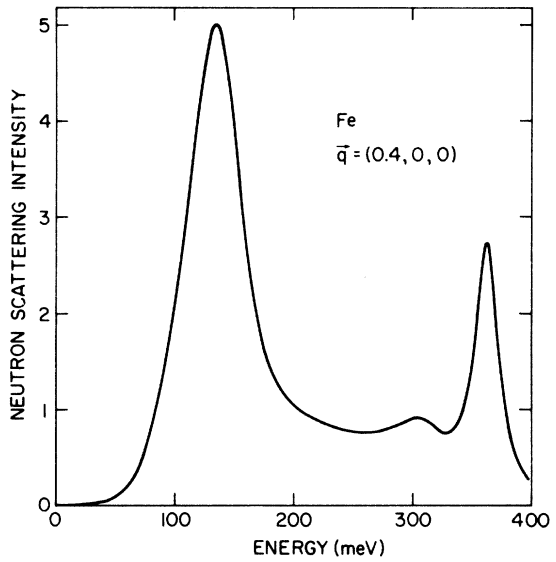

FIG. 7. Calculated spin-wave cross section for $\vec{q} = (0.4, 0, 0)$, as in Fig. 5 but the vertical scale adjusted so that the profile can be viewed. Note that in addition to the broad "acoustic" spin wave at 135 meV there is an additional "optical" spin-wave mode at 360 meV.

scattering at lower energies (on the scale of Fig. 5 the peak intensity coincides with the abscissa) and is surely unobservable in the experiments reported to date. Thus we would predict that the spin-wave scattering would become unobservable above ~100 meV, which agrees very well with experiment.[4] It is hoped that, with the advent of new neutron sources, this scattering can be observed. It would be particularly interesting to determine if the "optical" spin-wave mode, which has a dispersion ranging from 300 meV upward in the calculations, actually exists.

The calculated cross section for nickel is shown in Fig. 8 for $\vec{q}$ along [100]. These results differ from those for iron in that a remnant of the spin-wave peak appears to exist out to the zone boundary. In addition, two branches are clearly visible over part of the zone as is the case for iron. In the [111] direction, on the other hand, the spin-wave peak simply continues to decrease in intensity as $|\vec{q}|$ increases, and we would expect the spin-wave scattering to become unobservable above ~100 meV.

The spin-wave dispersion curve with $\vec{q}$ along [100] for nickel obtained from the band structure described in the previous section is shown by the curves in Fig. 9 labeled CD1. There are two branches, one "optic"

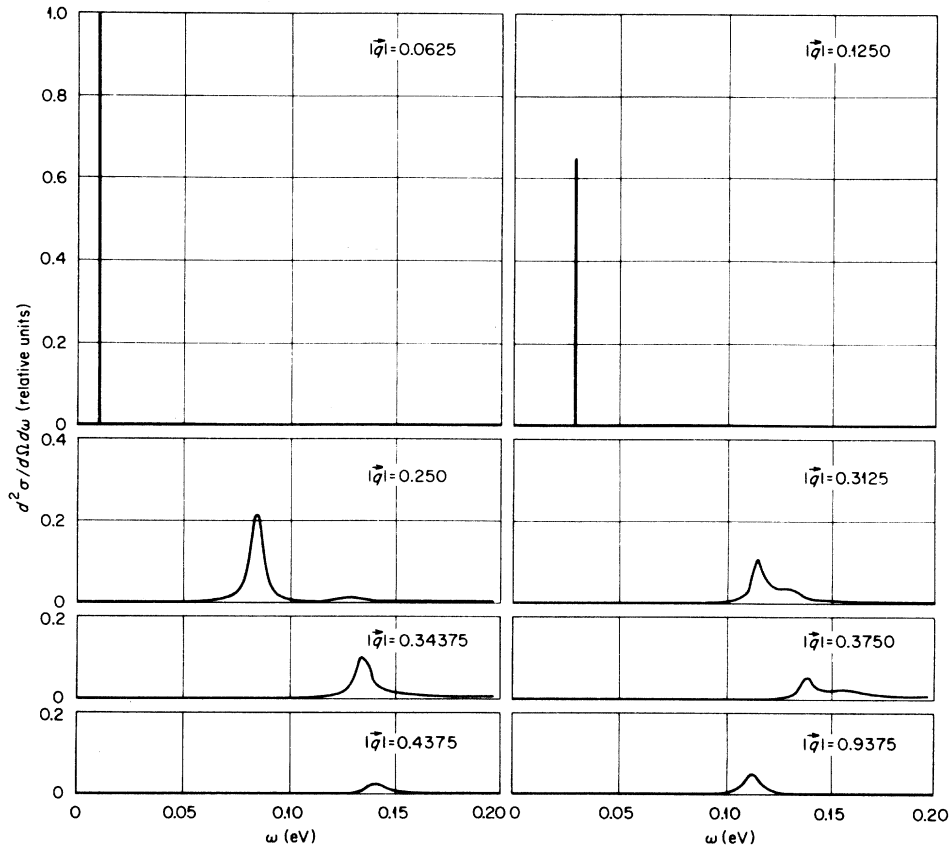

FIG. 8. Spin-wave scattering cross section for ferromagnetic nickel for various wave vectors (in units of $2\pi/a_0$) along [100].

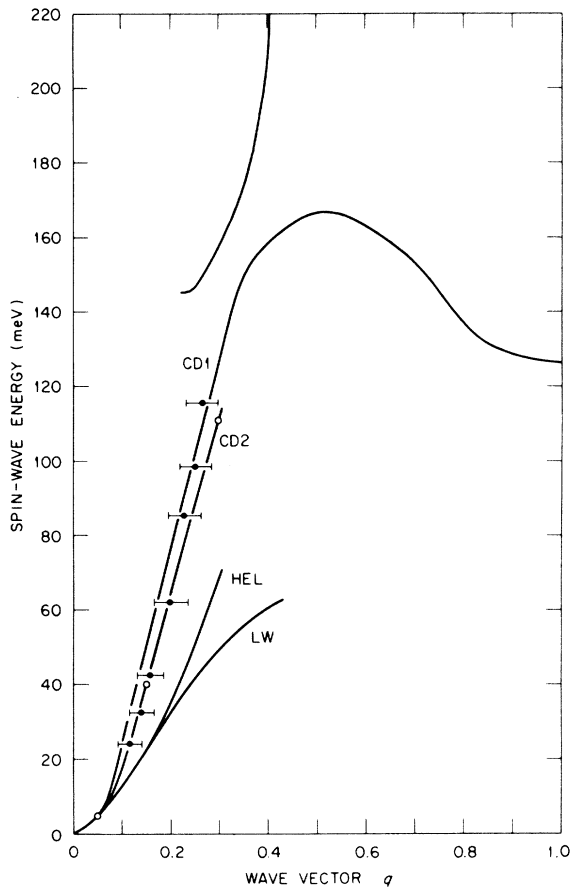

FIG. 9. Spin-wave dispersion curves for ferromagnetic nickel for various band structures and approximations. The experimental data are represented by the bars and from Ref. 3.

and one acoustic, which appear to interact. The reason the scattering vanishes in the optic branch as $q \rightarrow 0$ is because of the exact result given in Eq. (11) that all of the scattering must be in the acoustic mode. The agreement of this part of the dispersion curve with the experimental results[3] is clearly very good. In the region above 100 meV the [111] spin-wave peaks were found to broaden considerably. The dispersion curve obtained from these relatively weak peaks bent over (deviating from quadratic behavior) and then died out. The [111] dispersion curve is effectively identical to the [100] result for energies around 100 meV and below.

Part of the apparent discrepancy between theory and experiment along [100] was recently eliminated by a neutron experiment carried out by Mook.[30] The optical mode was indeed detected and was found to be in excellent agreement with the behavior predicted in Fig. 9. The bending over of the acoustic branch was detected but no evidence was found for the existence of a weak branch persisting out to the zone boundary.

The remainder of the curves plotted in Fig. 9 correspond to calculations carried out with different potentials and approximations. The dispersion curve labeled CD2 was obtained by slightly modifying the paramagnetic bands used in the calculation labeled CD1 in order to test the sensitivity of the calculation to small changes in the potential. The dispersion curve is practically unchanged and only the lower $\vec{q}$ part is drawn in.

The curve labeled HEL was obtained from a band structure which was shown by Hodges *et al.*[12] to be incorrect for nickel. This calculation demonstrates that if unreasonable band structures are used then we get poor agreement with experiment. Finally, the curve labeled LW was obtained from the enhanced-susceptibility–rigid-band-splitting model investigated by Lowde and Windsor[6] and was based on exactly the same set of paramagnetic bands used to generate the ferromagnetic bands for the CD1 calculation. The LW dispersion curve is then what one gets from the CD1 result if a constant-matrix-element approximation is used. Clearly the effect of including the band and wave-vector dependence of the matrix elements is essential.

Another important aspect of this improved matrix-element approximation is that it leads to a correct prediction of the disappearance of spin-waves in both nickel and iron. Here again the constant-matrix-element approximation falls short. In order to understand why this is the case we need to examine the theory in more detail.

V. SPIN-WAVE DISAPPEARANCE PHENOMENON

The disappearance of spin-waves can be understood in terms of a very simple argument. Spin-waves in the itinerant model correspond to a bound state between an electron of a given spin and a hole of opposite spin. Another type of magnetic excitation which exists in an itinerant magnet results from an electronic spin-flip excitation across the Fermi surface which creates single-particle electron-hole pair with opposite spin. Such excitations are called Stoner excitations. Spin-waves can, therefore, decay into Stoner excitations provided their energies are comparable and there is sufficient coupling. The spin-wave lifetime will depend on the details of the coupling between these excitations and on the density of Stoner excitations into which the spin-wave can decay.

In the constant-matrix-element approximation it is well known that the spin-wave lifetime ρ, which is inversely related to the width of the spin-wave peak, is proportional[6] to the total density of Stoner excitations for a given momentum transfer $\vec{q}$

$$\rho(\vec{q},\omega)=\frac{1}{N}\sum_{nm,\vec{k}}\delta(\omega-E(m\vec{k}+\vec{q}\uparrow)+E(n\vec{k}\downarrow)) \quad , \tag{28}$$

where $\delta(x)$ is the Dirac δ function. Since the bands are rigidly split in this approximation, ρ is nonzero only at the splitting parameter Δ, when $\vec{q}=0$:

$$\rho(\vec{q}=0,\omega)=\delta(\omega-\Delta) \quad . \tag{29}$$

As $|\vec{q}|$ increases from zero, $\rho(\vec{q},\omega)$ will be nonzero over some finite energy range. The region in q,ω space where $\rho(\vec{q},\omega)$ is nonzero is called the Stoner continuum and is shown schematically in Fig. 10, along with the spin-wave dispersion curve. This leads us to the conventional picture of the spin-waves disappearing as they run into the Stoner continuum.

We have carried out an extensive study of the Stoner density of states for nickel and iron which shows that this picture cannot be correct. An example of the type of results that we find is shown in Fig. 11. These particular results were obtained using our bands for nickel and are for $\vec{q}$ along [111]. The big contribution to $\rho(\vec{q},\omega)$ comes from the d-like bands, with the maximum occurring around the average d-symmetry-splitting parameter. The important point to be made here is that nothing very much oc-

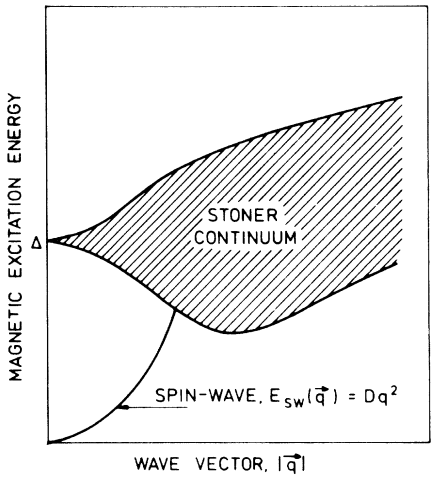

FIG. 10. Schematic representation of the magnetic excitation spectra for a single-band itinerant ferromagnet as based on a constant-matrix-element approximation.

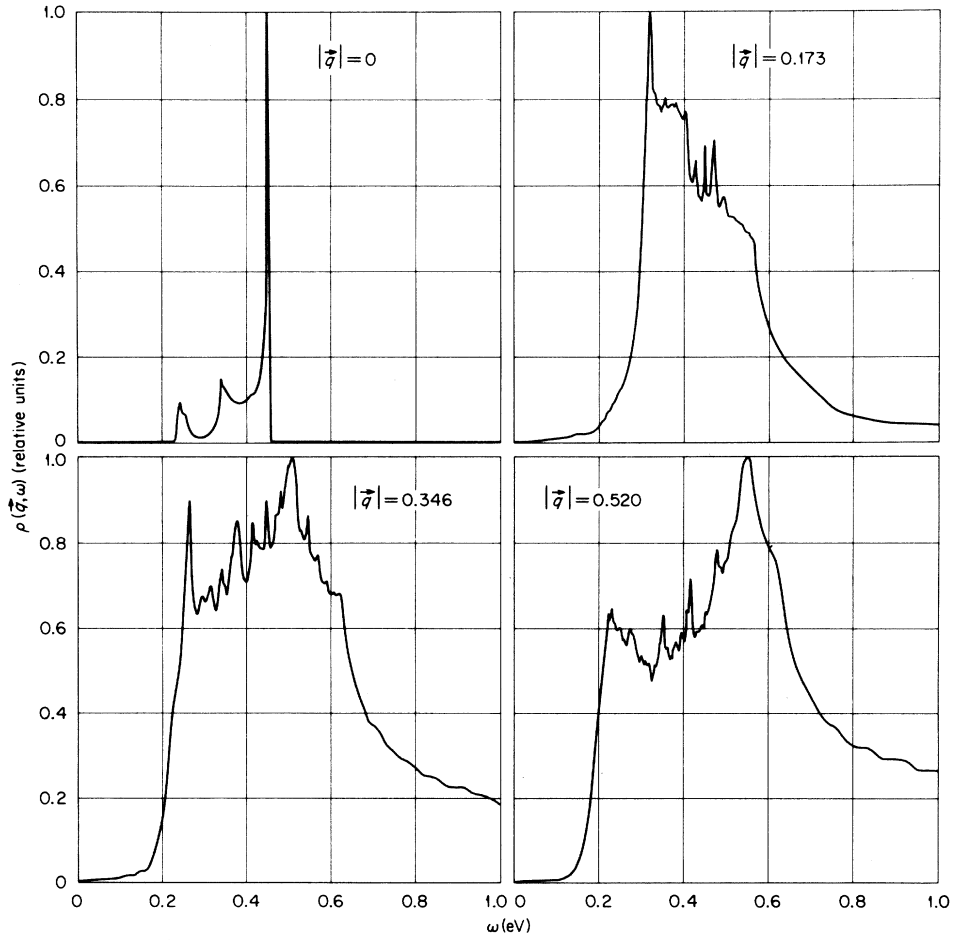

FIG. 11. Stoner band density of states for ferromagnetic nickel for various wave vectors (in units of $2\pi/a_0$) along [111].

curs in the region around 100 meV as we sweep through the range of wave vectors where the spin-wave should disappear. We also find that even if the large contribution to $\rho(\vec{q},\omega)$ is shifted down in energy (by arbitrarily lowering the d-symmetry-splitting parameter) there is still much too gradual a change in ρ with both q and ω to account for the sudden disappearance of the spin-waves observed in the neutron experiments. The discrepancy between the spin-wave disappearance and the high density of Stoner states is even more striking for iron, since the disappearance occurs at ~ 100 meV as in nickel but the band splitting is approximately 4 times as large ($\Delta \sim 2$ eV). A typical Stoner denstiy of states for iron is shown in Fig. 12. Qualitatively similar densities were obtained for different $\vec{q}$ and different potentials, with the only general trends noted that the spectra tended to be somewhat sharper at smaller $|\vec{q}|$, broader with larger Δ, and peaked around the value of the splitting. Even in the extreme case of $\Delta=0$ shown in the lower part of Fig. 12, the bulk of the Stoner density of states occurs at high energies, and the density is still not very large below ~ 100 meV. Of course for iron and nickel it is not correct even qualitatively to set $\Delta=0$ for $T > T_c$.

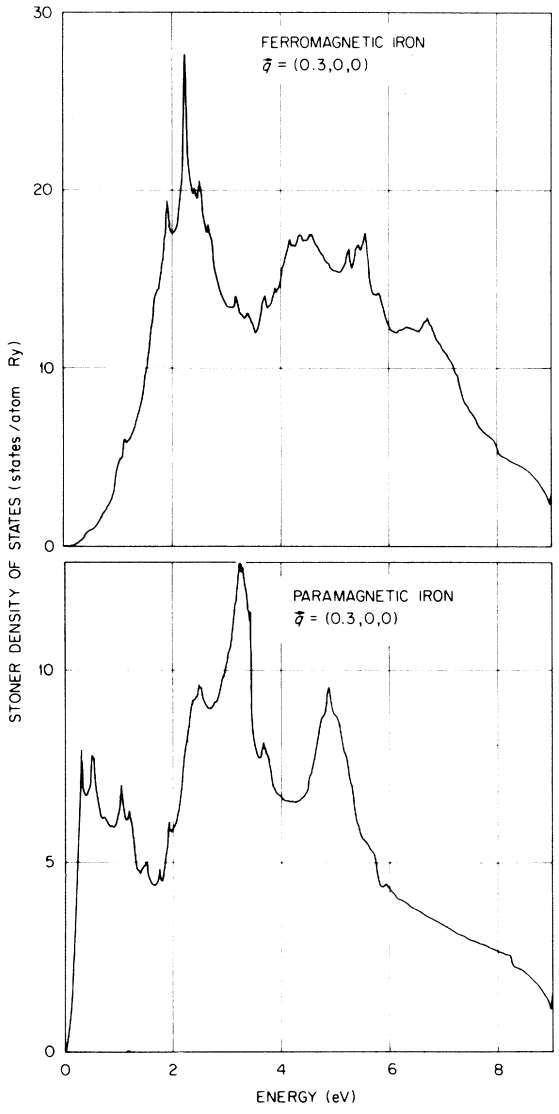

FIG. 12. Typical Stoner density of states calculated for iron with a band splitting of $\Delta=2.2$ eV (top) and $\Delta=0$ (bottom).

The situation is altered significantly when we introduce the band and wave-vector dependence of the matrix elements. In this case the expression for G_{sw} is quite complicated [see Eq. (24)] but by introducing the matrix which diagonalizes $(I+\Gamma W)$ it can be reduced to a form which is similar to the constant-matrix-element result. We can then identify the quantity which determines the spin-wave width. This function has the general form

$$\tilde{\rho}(\vec{q},\omega)=\frac{1}{N}\sum_{nm,\vec{k}} K(n,m,\vec{k},\vec{q},\omega) \times \delta(\omega - E(m\vec{k}+\vec{q}\uparrow)+E(n\vec{k}\downarrow)) \ , \tag{30}$$

where K is a complicated but well-defined function of the wave-vector expansion coefficients and elements of the diagonalization matrix. This function can be viewed as a weighted density of Stoner excitations.

Numerical calculations of $\tilde{\rho}$ clearly indicate why the spin-wave peak disappears. Results from such a calculation for iron are shown in Fig. 13. The criterion which controls the spin-wave linewidth is the value of $\tilde{\rho}$ in the immediate vicinity of the spin-wave pole.

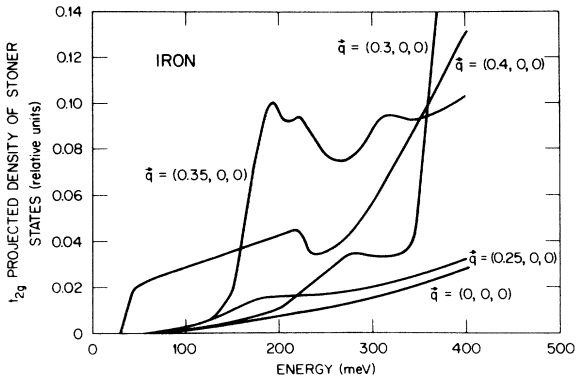

FIG. 13. Weighted density of Stoner states for ferromagnetic iron for various wave vectors (in units of $2\pi/a_0$) along [100]. The width of the spin wave is determined by the magnitude of $\tilde{\rho}$ in the vicinity of the spin-wave pole (see Fig. 6). Note that around 100 meV the magnitude of $\tilde{\rho}$ increases abruptly for q between 0.35 and 0.4, and this causes a large increase in the spin-wave linewidth (see Figs. 5 and 7). The total Stoner density of states shows no significant change in this region.

We see that between $q = 0.35$ and 0.40 $\tilde{\rho}$ increases dramatically (at ~ 100 meV), and this in turn broadens the spin-wave width. The total Stoner density of states on the other hand shows no structure in this energy range but rather is just a monotonically increasing function of energy which is weakly dependent on q. It is, therefore, a rather complicated weighted density of Stoner states that controls the disappearance phenomena and *not* the total density ($K \equiv 1$). These calculations also show that there is a nonzero width to the spin-wave line at all nonzero q. The widths, of course, are small for small q. The simple picture given in Fig. 10 is, therefore, still valid provided we view the shaded region as the region of a high density of appropriately weighted Stoner excitations.

VI. CONCLUSIONS

An approximate method for calculating dynamic properties of an itinerant ferromagnet has been described and numerically investigated. This method is based on a Green's-function approach with RPA decoupling. The general RPA equations have been solved using an approximate method for including the band and wave-vector dependence of relevant matrix elements. This improved solution of the RPA equations leads to a band- and wave-vector-dependent splitting of the energy bands, optic spin-wave modes, and an alternate view of the spin-wave disappearance phenomenon.

First-principles (zero-parameter) numerical calculations of the dynamic properties of nickel and iron have been found to be in excellent agreement with neutron scattering experiments. These calculations not only yielded the correct dispersion relation and correctly described the measured disappearance phenomena but predicted the existence of an optical spin-wave branch in nickel which was subsequently observed. These numerical results were found to be essentially independent of the explicit spin dependence of the electron wave function.

The results presented in this paper clearly indicate that the itinerant-electron model of magnetism provides not only the correct qualitative description but also a good quantitative description of the low-temperature dynamic properties of transition-metal magnets. The extension of these calculations to finite temperature cannot be carried out at present because of the absence of a realistic finite-temperature theory. This very difficult problem is currently under investigation.

ACKNOWLEDGMENT

Research sponsored by the Division of Materials Sciences, U.S. Department of Energy under Contract No. W-7405-eng-26 with the Union Carbide Corporation.

---

*Dept. of Physics, University of Maryland, College Park, Md. 20742.

[1]See, for example, the review by C. Herring, in *Magnetism*, edited by G. T. Rado and H. Suhl (Academic, New York, 1966), Vol. IV.

[2]T. Izuyama, D. Kim, and R. Kubo, J. Phys. Soc. Jpn. 18, 1025 (1963).

[3]H. A. Mook, R. M. Nicklow, E. D. Thompson, and M. K. Wilkinson, J. Appl. Phys. 40, 1450 (1969); H. A. Mook, J. W. Lynn, and R. M. Nicklow, Phys. Rev. Lett. 30, 556 (1973); in *Proceedings of the Ninteenth Conference on Magnetism and Magnetic Materials, Boston, 1973*, edited by C. D. Graham, Jr. and J. J. Rhyne, AIP Conf. Proc. No. 18 (AIP, New York, 1974), p. 781.

[4]H. A. Mook and R. M. Nicklow, Phys. Rev. B 1, 336 (1973); J. W. Lynn, *ibid.* 11, 2624 (1975).

[5]E. D. Thompson, Phys. Rev. Lett. 19, 635 (1967).

[6]R. D. Lowde and C. G. Windsor, Adv. Phys. 19, 813 (1970).

[7]J. F. Cooke, Phys. Rev. B 7, 1108 (1973).

[8]J. F. Cooke and H. L. Davis, in *Proceedings of the Eighteenth Conference on Magnetism and Magnetic Materials, Denver, 1972*, edited by C. D. Graham, Jr. and J. J. Rhyne, AIP Conf. Proc. No. 10 (AIP, New York, 1975), p. 1218; J. F. Cooke, J. W. Lynn, and H. L. Davis, Solid State Commun. 20, 799 (1976); in *Proceedings of the Twentieth Conference on Magnetism and Magnetic Materials, San Francisco, 1974*, edited by C. D. Graham, Jr., G. H. Lander, and J. J. Rhyne, AIP Conf. Proc. No. 24 (AIP, New York, 1974), p. 329.

[9]W. Marshall and S. W. Lovesey, *Theory of Thermal Neutron Scattering*, (Oxford Univ. Press, Oxford, 1971).

[10]F. S. Ham and B. Segall, Phys. Rev. 124, 1786 (1961).

[11]V. L. Moruzzi, J. F. Janak, and A. R. Williams, *Calculated Electronic Properties of Metals* (Pergamon, New York, 1978).

[12]L. Hodges, H. Ehrenreich, and N. D. Lang, Phys. Rev. 152, 505 (1966).

[13]J. C. Slater and G. F. Koster, Phys. Rev. 94, 1498 (1954).

[14]H. Daman, A. Herr, and A. J. P. Meyer, J. Appl. Phys. 39, 669 (1968).

[15]G. G. Scott, Rev. Mod. Phys. 34, 102 (1962).

[16]H. A. Mook, Phys. Rev. 148, 495 (1966).

[17]C. G. Shull, in *Electronic Structure and Alloy Chemistry of the Transition Elements*, edited by P. A. Beck (Interscience, New York, 1963), p. 15; C. G. Shull and H. A. Mook, Phys. Rev. Lett. 16, 184 (1966); C. G. Shull and Y. Yamada, J. Phys. Soc. Jpn. Suppl. B-III 17, 1 (1962).

[18]G. M. Stocks, R. W. Williams, and J. S. Faulkner, Phys. Rev. B 4, 4390 (1971).

[19]H. Ehrenreich and L. Hodges, in *Methods in Computational Physics*, edited by B. Adler, S. Fernbach, and M. Roten-

berg (Academic, New York, 1968), p. 149–192.
[20]For example, see Ref. 11.
[21]D. E. Eastman, F. J. Himpsel, and J. A. Knapp, J. Appl. Phys. 50, 1950 (1979).
[22]J. H. Wood, Phys. Rev. 126, 517 (1962).
[23]A. V. Gold, L. Hodges, P. T. Panousis, and D. R. Stone, Int. J. Magn. 2, 357 (1971).
[24]L. F. Mattheiss, Phys. Rev. 134, A970 (1964).
[25]H. L. Davis, unpublished results concerning a potential for paramagnetic iron generated using wave functions from C. F. Fischer, University of British Columbia Report, January 1968 (unpublished). To generate this potential, Fisher's Fe wave functions for Fe $3d^6 4s^2$ were constrained to be in a configuration $3d^7 4s^1$.
[26]K. J. Duff and T. P. Das, Phys. Rev. B 3, 192 (1971).
[27]S. Wakoh and J. Yamashita, J. Phys. Soc. Jpn. 21, 1712 (1966).
[28]G. Gilat and L. J. Raubenheimer, Phys. Rev. 144, 390 (1966).
[29]G. Lehmann and M. Taut, Phys. Status Solidi 54, 469 (1972).
[30]H. A. Mook (unpublished).